Fourier Transform Infrared Difference Spectroscopy of Photosystem II Tyrosine D Using Site-Directed Mutagenesis and Specific Isotope Labeling†

Rainer Hienerwadel,‡,§ Alain Boussac,‖ Jacques Breton,‡ Bruce A. Diner,⊥ and Catherine Berthomieu*,‡

Section de Bioénergétique, CEA-Saclay, 91191 Gif-sur-Yvette Cedex, France, and Central Research and Development Department, Experimental Station, E. I. du Pont de Nemours & Company, Wilmington, Delaware 19880-0173

Received June 24, 1997; Revised Manuscript Received September 25, 1997⊗

ABSTRACT: Tyrosine D (Tyr_D), a side path electron carrier of photosystem II (PS II), has been studied by light-induced Fourier transform infrared (FTIR) difference spectroscopy in PS II core complexes of *Synechocystis* sp. PCC 6803 using the experimental conditions previously optimized to generate the pure $Tyr_D^{\bullet}/Tyr_D$ FTIR difference spectrum in PS II-enriched membranes of spinach [Hienerwadel, R., Boussac, A., Breton, J., and Berthomieu, C. (1996) *Biochemistry 35*, 115447−115460]. IR modes of Tyr_D and $Tyr_D^{\bullet}$ have been identified by specific ^2H- or ^{13}C-labeling of the tyrosine side chains. The υ_{8a}(CC) and υ_{19}(CC) IR modes of Tyr_D are identified at 1615 and 1513−1510 cm^{-1}, respectively. These frequencies show that Tyr_D is protonated. Comparison of isotope-sensitive signals *in situ* with those of the model compound *p*-methylphenol dissolved in different solvents leads to the assignment of the $\upsilon_{7'a}$(CO) and δ(COH) modes of Tyr_D at 1275 and 1250 cm^{-1}, respectively. It is shown that these modes and in particular the δ(COH) IR mode are very sensitive to the formation of hydrogen-bonded complexes with amide C═O or with imidazole nitrogen atoms. The frequencies observed *in situ* show that Tyr_D is hydrogen-bonded to the imidazole ring of a neutral histidine. For the radical $Tyr_D^{\bullet}$, isotope-sensitive IR modes are identified at 1532 and 1503 cm^{-1}. The signal at 1503 cm^{-1} is assigned to the υ(CO) mode of $Tyr_D^{\bullet}$ since it is sensitive to ^{13}C-labeling at the ring carbon involved in the C4−O bond. The perturbation of Tyr_D and $Tyr_D^{\bullet}$ IR modes upon site-directed replacement of D2-His189 by Gln confirms that a hydrogen bond exists between both Tyr_D and $Tyr_D^{\bullet}$ and D2-His189. In the D2-His189Gln mutant, the $\upsilon_{7'a}$(CO) mode of Tyr_D at 1267 cm^{-1} and the δ(COH) mode at ≈1228 cm^{-1} show that a hydrogen bond is formed between Tyr_D and an amide carbonyl, probably that of the D2-Gln189 side chain. Electron nuclear double resonance (ENDOR) measurements have shown that $Tyr_D^{\bullet}$ is hydrogen-bonded in the wild type but not in the mutant [Tang, X.-S., Chrisholm, D. A., Dismukes, G. C., Brudwig, G. W., and Diner, B. A. (1993) *Biochemistry 32*, 13742−13748]. The υ(CO) mode of $Tyr_D^{\bullet}$ at 1497 cm^{-1} is downshifted by 6 cm^{-1} compared to WT PS II, indicating that hydrogen bonding induces a frequency upshift of the υ(CO) IR mode of $Tyr^{\bullet}$. IR signals from the Gln side chain υ(C═O) mode are proposed to contribute at 1659 and 1692 cm^{-1} in the Tyr_D and $Tyr_D^{\bullet}$ states, respectively. These frequencies are consistent with the rupture of a hydrogen bond upon $Tyr_D^{\bullet}$ formation in the mutant. The frequency of the υ(CO) mode of $Tyr_D^{\bullet}$, observed at 1503 cm^{-1} for WT PS II, is intermediate between that observed at 1497 cm^{-1} in the D2-His189Gln mutant and at 1513 cm^{-1} for $Tyr^{\bullet}$ formed by UV irradiation in borate buffer, suggesting weaker or fewer hydrogen bonds for $Tyr_D^{\bullet}$ in PS II than in solution. The role of D2-His189 in proton uptake upon $Tyr_D^{\bullet}$ formation is also investigated.

Photosystem II (PS II)[1] of green plants drives the light-induced reduction of plastoquinone (PQ to PQH_2) and the oxidation of water to molecular oxygen. This photosystem also contains two redox-active tyrosines, Tyr_D and Tyr_Z, which were identified as such by EPR studies of preparations of *Synechocystis* sp. PCC 6803 containing isotopically labeled tyrosine (*1*, *2*). Site-directed mutagenesis experiments have shown that Tyr_D and Tyr_Z occupy homologous positions within the homologous polypeptides D2 (D2-160, amino acid numbering for *Synechocystis* sp. PCC 6803; *3*, *4*) and D1 (D1-161; *5*, *6*) that constitute the dimeric core of PS II. For both tyrosines, oxidation results in the formation of neutral radicals with very similar EPR spectra (see ref *7* for a review). Tyr_Z forms a transient radical and is directly

† R.H. was supported by an EC fellowship (ERB40016T933365). B.A.D. gratefully acknowledges grant support from the NRICGP/USDA.

* Corresponding author: e-mail berthomieu@dsvidf.cea.fr; Fax 33 1 69 08 87 17.

‡ CEA-Saclay.

§ Present address: Laboratoire de Biophysique des Transporteurs d'Electrons, Case 901, Université d'Aix-Marseille II, 163 Avenue de Luminy, 13288 Marseille Cedex, France.

‖ URA CNRS 2096.

⊥ DuPont.

⊗ Abstract published in *Advance ACS Abstracts,* November 15, 1997.

[1] Abbreviations: PS II (I), photosystem II (I); RC, reaction center; D1 and D2, polypeptides of PS II; Tyr_D, tyrosine D2−160; Tyr_Z, tyrosine D1−161; P_{680} (P_{700}), primary chlorophyll electron donor of PS II (PS I); Q_A, primary electron acceptor plastoquinone; Fe, non-heme iron cofactor of PS II; WT, wild type; PQ, plastoquinone; Chl, chlorophyll; *p*-cresol, *p*-methylphenol; Tris, tris(hydroxymethyl)aminomethane; DMF, *N*,*N*′-dimethylformamide; 1MeIm (4MeImH), 1- (4-) methylimidazole; $^2H_4$-Tyr, tyrosine with deuterated ring; $^{13}C_6$-Tyr, tyrosine with all six ring carbons ^{13}C-labeled; $^{13}C_1$(4)-Tyr, tyrosine ^{13}C-labeled at the ring carbon C4 binding to the hydroxyl group; [U-^{13}C]-His, fully ^{13}C-labeled histidine; ν, stretching vibration; δ, bending vibration; FTIR, Fourier transform infrared; EPR, electron paramagnetic resonance; ESEEM, electron spin echo envelope modulation; ENDOR, electron nuclear double resonance; TRIPLE, electron−nuclear−nuclear triple resonance; RR, resonance Raman.

S0006-2960(97)01521-3 CCC: $14.00

involved in electron transfer reactions leading to oxygen evolution. In contrast, Tyr_D forms a dark-stable radical, the physiological function of which is not as yet clearly understood. The radicals also differ by their reduction potentials (*8*−*10*), their accessibility to exogenous reductants, and the position and flexibility of their aromatic rings with respect to the β-methylene protons of the tyrosine alkyl chain (*11*−*13*). The presence of a hydrogen bond to both tyrosine radicals has been proposed, although that to $Tyr_Z^{\bullet}$ appears to be more heterogeneous than that to $Tyr_D^{\bullet}$ (*14*−*20*). There is magnetic resonance evidence that the side chain of His D2-189 is involved in the hydrogen bond to $Tyr_D^{\bullet}$ and it was proposed that His D2-189 could be the proton acceptor upon $Tyr_D^{\bullet}$ radical formation (*3*, *17*, *20*−*23*). The implication of the homologous histidine residue on D1 (190) in a hydrogen bond to $Tyr_Z^{\bullet}$ and/or as proton acceptor is still controversial (*19*, *24*−*26*). More generally, the specific role of the amino acids surrounding Tyr_Z and Tyr_D in tuning the redox and functional properties of the tyrosines is not clearly understood.

The sensitivity of the vibrational modes of molecules to structural perturbations and interactions, as well as the nonselectivity of IR spectroscopy, explain that light-induced FTIR difference spectroscopy is an attractive method to identify the different chemical groups involved in hydrogen-bond formation or proton transfer reactions (method reviewed in ref *27*). Cofactors and protein residues perturbed by the light-induced reaction will be detected directly by their specific vibrational modes. FTIR difference spectra corresponding to the change of redox state of a single cofactor of PS II on the electron donor side or on the acceptor side are a prerequisite for reliable assignment of the IR bands. They are obtained using brief illumination of samples in the presence of exogenous electron donors or acceptors (*28*−*32*). Experimental conditions have been optimized to generate pure FTIR difference spectra corresponding to Tyr_D photooxidation in Mn-depleted PS II-enriched membranes of spinach (*32*). From the comparison of the $Tyr_D^{\bullet}/Tyr_D$ FTIR spectrum with FTIR difference spectra obtained upon UV irradiation of *p*-methylphenol (*p*-cresol) at 10 K, we proposed that the ν(CO) mode of $Tyr_D^{\bullet}$ contributes at 1504 cm^{-1} for spinach PS II (*32*).

In the present work, IR modes of Tyr_D and $Tyr_D^{\bullet}$ are identified in *Synechocystis* sp. PCC 6803 by comparison of light-induced $Tyr_D^{\bullet}/Tyr_D$ FTIR difference spectra recorded in the presence of unlabeled or specifically ^{13}C- ($^{13}C_6$-Tyr) and ^{2}H- ($^{2}H_4$-Tyr) ring-labeled tyrosines and also tyrosine ^{13}C-labeled at the C4 ring carbon [$^{13}C_1$(4)-Tyr]. The interactions of Tyr_D and $Tyr_D^{\bullet}$ with His D2-189 are investigated using WT PS II cores with fully ^{13}C-labeled histidines ([U-^{13}C]His) and PS II cores from the D2-His189Gln mutant grown in the presence of either unlabeled or $^{2}H_4$-labeled tyrosine. It was previously shown that the D2-His189Gln mutant lacks a hydrogen bond to $Tyr_D^{\bullet}$ (*17*, *20*, *22*, *23*). Thus the comparison of the WT and the mutant PS II cores allows a direct measure of the influence of hydrogen bonding on the vibrational modes of $Tyr_D^{\bullet}$.

MATERIALS AND METHODS

Mn-depleted PS II core complexes were isolated according to Rögner et al. (*33*) with the modifications described in Tang et al. (*19*) from the glucose-tolerant (*34*) and phycocyanin-deficient "olive" strain (*33*) of the cyanobacterium *Synechocystis* sp. PCC 6803 wild type (WT) or D2-His189Gln mutant. The isolation of the mutant has been previously described (*17*). For the specific $^{13}C_6$-, $^{13}C_1$(4)-, and $^{2}H_4$-labeling of tyrosines, the cyanobacteria were grown photoautotrophically for 6−7 days in BG-11 medium (*35*) containing 0.5 mM phenylalanine, 0.25 mM tryptophan, and 0.25 mM isotopically labeled tyrosine, according to the method of Barry and Babcock (*1*). Control PS II preparations were made from cyanobacteria grown in the presence of unlabeled aromatic amino acids. The histidine-tolerant strain selected in ref *36* was used for the specific labeling of histidine, and the cyanobacteria were grown in the presence of either unlabeled (control) or U-^{13}C-labeled histidine, as previously described (*36*). The labeled amino acids (98% isotope enriched) were purchased from Cambridge Isotope Laboratories.

Detergent-solubilized PS II cores (30−35 μg of chlorophyll) were used for each IR sample in the FTIR investigation of Tyr_D photooxidation. The PS II cores were incubated in 300 μL of sodium phosphate buffer (50 mM) at pH 6 in the presence of sodium formate (50 mM) for about 3 h at 4 °C. Then, the sample was concentrated to about 7 μL using a Microcon 30 (Amicon). To prepare the IR sample, 3.5 μL of a 0.5 M ferricyanide solution was dried onto a CaF_2 window. The concentrated *Synechocystis* sp. PCC 6803 PS II core suspension was then deposited on the window and partially dried under a nitrogen gas stream. The sample was then squeezed to the final path length using a second CaF_2 window. Experiments were performed at 4 °C using a water-cooled sample wheel allowing dark adaptation of several samples. FTIR difference spectra were obtained by recording 80 scans (corresponding to ≈14 s) before and 2 s after a 1-s illumination of the sample. Illumination was performed with a 680-nm continuous laser diode of 20 mW output (Laser-Max Inc.). FTIR difference spectra obtained with either a single laser flash or with the 1-s illumination were indistinguishable, except that the latter illumination gave larger signals. The spectra were recorded during ≈20 h, with dark periods of ≈15 min between successive illuminations. No alteration of the shape of the FTIR difference signals was observed during data acquisition. Spectra obtained with 10−15 samples were averaged. FTIR spectra were recorded with 4 cm^{-1} resolution on a Bruker IFS 88 spectrometer equipped with a MCT-A detector.

RESULTS

$Tyr_D^{\bullet}/Tyr_D$ FTIR Spectra of Wild-Type PS II Preparations. Spectrum A in Figure 1 shows the $Tyr_D^{\bullet}/Tyr_D$ FTIR difference spectrum recorded in Mn-depleted PS II core preparations of the cyanobacterium *Synechocystis* sp. PCC 6803. The same experimental conditions as in Mn-depleted PS II-enriched membranes of spinach (Figure 1B; *32*) were used to record the $Tyr_D^{\bullet}/Tyr_D$ spectrum free of contributions from other redox intermediates, e.g., the electron acceptor plastoquinone Q_A and a secondary electron donor chlorophyll (Chl). The inset of Figure 1A shows the 2200−1900-cm^{-1} region of spectrum A, where the ν(C≡N) IR mode of ferricyanide appears as a negative signal at 2116 cm^{-1} and where ferrocyanide contributes a positive band at 2036 cm^{-1}. This indicates that ferricyanide is reduced upon illumination and functions as an efficient electron acceptor from Q_A^-. Accordingly, both spectra in Figure 1 lack the positive signal

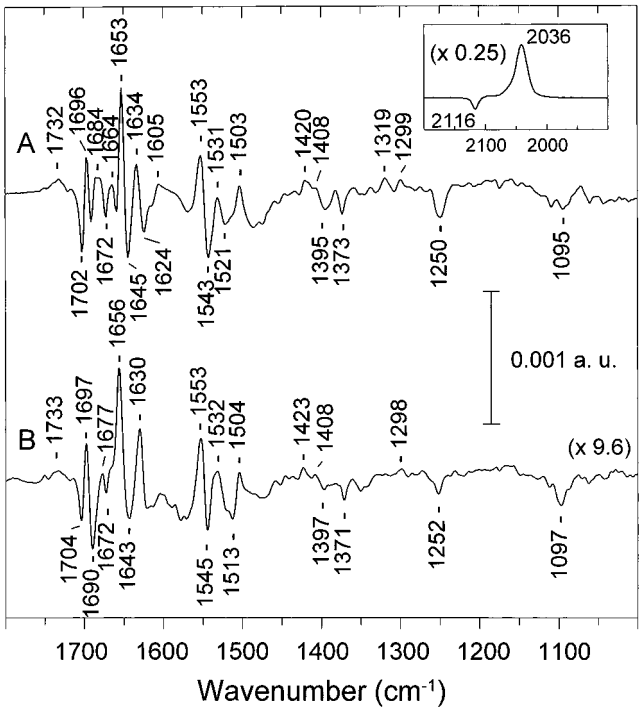

FIGURE 1: $Tyr_D^{\bullet}/Tyr_D$ FTIR difference spectra recorded in phosphate buffer, pH 6, in the presence of 50 mM formate and ferricyanide at 4 °C, 4 cm^{-1} resolution. (A) Mn-depleted PS II core preparation from *Synechocystis* sp. PCC 6803 WT, 92 160 scans; inset, 2200−1900 cm^{-1} region of the $Tyr_D^{\bullet}/Tyr_D$ spectrum, (B) Mn-depleted PS II-enriched membranes of spinach, 374 400 scans.

at 1478 cm^{-1}, which was previously demonstrated to be characteristic of the Q_A^-/Q_A FTIR spectrum (*28*, *30*, *32*; see also *37*) and proposed to account for the ν(CO) mode of semiquinone Q_A^- (*28*, *30*). Also, a $Tyr_D^{\bullet}/Tyr_D$ UV−vis difference spectrum free from contributions from Chl oxidation or Q_A reduction is obtained by flash illumination on *Synechocystis* core samples in the same buffer as used for FTIR spectroscopy (*38*). Therefore, the spectra of Figure 1 show the changes in structure and interactions of Tyr_D upon radical formation and the rearrangement of chemical groups, amino acids, and cofactors of PS II that are perturbed by the formation of $Tyr_D^{\bullet}$. The negative signals correspond to the Tyr_D state, the positive ones to the $Tyr_D^{\bullet}$ state.

The $Tyr_D^{\bullet}/Tyr_D$ FTIR difference spectra recorded either with *Synechocystis* sp. PCC 6803 (Figure 1A) or with spinach (Figure 1B) present a large number of common signals at almost the same frequencies in the whole spectral range. Differential bands appear at 1653(1656)/1645(1643)/1634(1630) cm^{-1} and 1553/1543(1545)/1531(1532) cm^{-1} for *Synechocystis* sp. PCC 6803 (spinach) in the amide I and II regions, respectively, where peptide IR modes are expected to contribute [Figure 1A(B), ref *39* and references therein]. This similarity suggests that microstructural changes of the peptide backbone, at the level of the tyrosine and/or of nearby amino acids, are conserved in both organisms upon $Tyr_D^{\bullet}$ formation. A positive band at 1732(1733) cm^{-1}, in the absorption region of protonated carboxylic group(s), a differential signal at 1702(1704)/1696(1697) cm^{-1}, and fingerprint signals in the 1530−1100 cm^{-1} region, positive at 1503(1504), 1420(1423)−1408, and 1299(1298) cm^{-1}, negative at 1513−1521, 1395(1397), 1373(1371), and 1250-(1252) cm^{-1} are also common to both spectra. The main spectral differences consist of a strong negative signal at 1690 cm^{-1} and a larger amplitude of the 1656-cm^{-1} band in the $Tyr_D^{\bullet}/Tyr_D$ spectrum recorded with spinach PS II and by the presence of a negative signal at 1624 cm^{-1} and of a small positive one at 1319 cm^{-1} for *Synechocystis* sp. PCC 6803 (Figure 1).

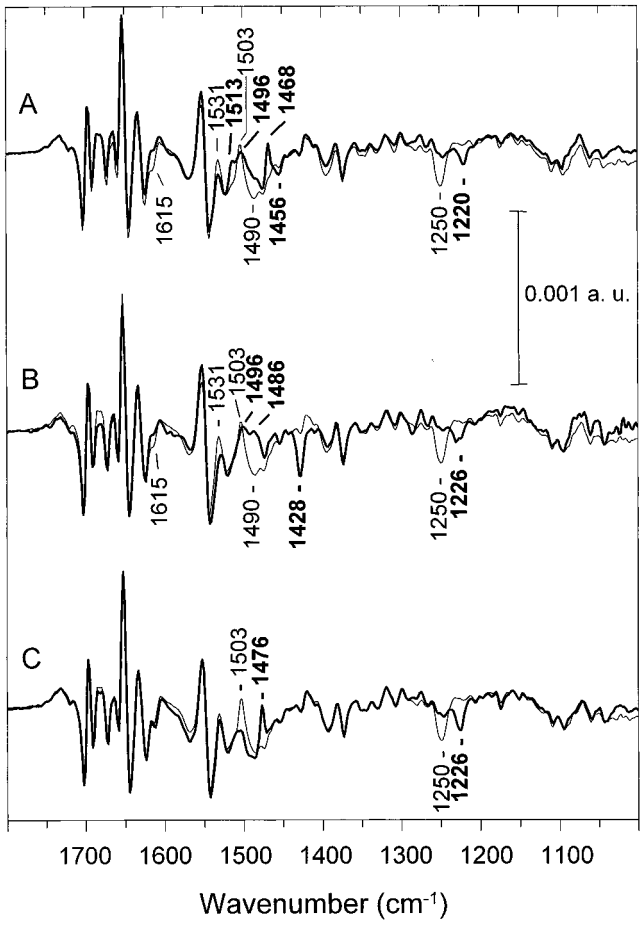

FIGURE 2: $Tyr_D^{\bullet}/Tyr_D$ spectra recorded using PS II cores from WT PS II grown in the presence of unlabeled amino acid (thin line, 107 840 scans) superimposed on the $Tyr_D^{\bullet}/Tyr_D$ spectra obtained using cores from WT cultures supplemented with (A) bold line, $^{13}C_6$-Tyr, 101 200 scans; (B) bold line, $^2H_4$-Tyr, 131 520 scans; or (C) bold line, $^{13}C_1(4)$-Tyr, 64 320 scans; 4 cm^{-1} resolution, 4 °C.

$Tyr_D^{\bullet}/Tyr_D$ Spectra Using Selectively Labeled Tyrosines. To identify the IR side chain modes of Tyr_D and $Tyr_D^{\bullet}$, we compare in Figure 2 the $Tyr_D^{\bullet}/Tyr_D$ FTIR spectra recorded with PS II cores isolated from *Synechocystis* sp. PCC 6803 cultures supplemented with aromatic amino acids either with unlabeled tyrosine (thin line) or with tyrosines in which the aromatic ring is selectively ^{13}C-labeled ($^{13}C_6$-Tyr, spectrum A bold line) or ^2H-labeled ($^2H_4$-Tyr, spectrum B bold line) or ^{13}C labeled only at the ring C4 carbon binding the Tyr hydroxyl [$^{13}C_1(4)$-Tyr, spectrum C bold line].

While the superimposed $Tyr_D^{\bullet}/Tyr_D$ spectra of Figure 2 are very similar, i.e., reproducible, above 1630 cm^{-1} and below 1200 cm^{-1}, the tyrosine side-chain labeling induces not only intensity changes but also clear band shifts in the spectral ranges 1630−1400 and 1300−1200 cm^{-1} (Figure 2A−C). This is illustrated by the negative band at 1250 cm^{-1} (Figure 2A, thin line), which is downshifted to 1220 cm^{-1} upon $^{13}C_6$ Tyr labeling (Figure 2A, bold line) or to 1226 cm^{-1} upon $^2H_4$ and $^{13}C_1(4)$ Tyr labeling (Figure 2B,C, bold line). The signal at 1250 cm^{-1} can thus be confidently assigned to a mode of unlabeled Tyr_D. The major bands

that are affected by the isotopic substitution of Tyr are comparable in amplitude to the other signals of the $Tyr_D^{\bullet}/Tyr_D$ spectrum observed below 1530 cm^{-1} or above 1700 cm^{-1}, i.e., in the absorption region of amino acid side chain modes. They are small as compared to the largest signals of the $Tyr_D^{\bullet}/Tyr_D$ spectrum at 1702/1696, 1653/1645, and 1553/1543 cm^{-1} (Figure 1A). The latter two sharp differential signals most probably correspond to the ν(C═O) (amide I) and ν(C═N) + δ(N−H) (amide II) vibrations of one or more peptide group(s). For peptidic ν(C═O) modes, absorption coefficients (ϵ) of 700 ± 100 and up to 980 ± 40 $L{\cdot}mol^{-1}{\cdot}cm^{-1}$ have been reported for α-helical and β-structures, respectively (*39*), while an ϵ of 430 ± 20 $L{\cdot}mol^{-1}{\cdot}cm^{-1}$ has been reported for the most intense mode of the Tyr side chain at 1518 cm^{-1} (*40*). Therefore, the amplitudes of the changes observed in the $Tyr_D^{\bullet}/Tyr_D$ spectra in Figure 2 are compatible with those expected for isotopic labeling of Tyr side chain.

$^{13}C_6$ Labeling. In the 1630−1400-cm^{-1} region, the $Tyr_D^{\bullet}/Tyr_D$ FTIR spectrum recorded in the presence of $^{13}C_6$-Tyr (Figure 2A, bold line) shows modified signal amplitudes at 1615, 1531, 1513, 1503, 1490, and 1456 cm^{-1}. A new sharp positive band appears at 1468 cm^{-1}, which can be assigned to $^{13}C_6$-$Tyr_D^{\bullet}$ (Figure 2A, bold line). In the 1550−1450-cm^{-1} spectral region, isotope-sensitive modes of Tyr_D (negative) and of $Tyr_D^{\bullet}$ (positive) are probably superimposed, as observed for the model compound *p*-cresol (*32*).

$^{2}H_4$ Labeling. Reproducible changes in signal intensity are observed at 1615, 1531, 1503, and 1490 cm^{-1} in the $Tyr_D^{\bullet}/Tyr_D$ spectrum, upon $^{2}H_4$-Tyr labeling (Figure 2B). Similar changes are also observed at these frequencies in Figure 2A upon $^{13}C_6$-Tyr labeling. This suggests contribution of unlabeled Tyr_D or $Tyr_D^{\bullet}$ at these frequencies. A positive band at 1486 cm^{-1} and a negative one at 1428 cm^{-1} in Figure 2B (bold line) are specific for the $Tyr_D^{\bullet}/Tyr_D$ spectrum recorded with PS II with $^{2}H_4$-Tyr and are thus assigned to $^{2}H_4$-$Tyr_D^{\bullet}$ and $^{2}H_4$-Tyr_D, respectively.

$^{13}C_1$(4) Labeling. The $^{13}C_1$(4) Tyr labeling is expected to greatly modify the frequency of the modes corresponding to vibrations at the C4−O bond of Tyr_D or $Tyr_D^{\bullet}$, while the other side-chain modes of Tyr_D should be only slightly perturbed (see below, Figure 4D). Only two differences appear between the $Tyr_D^{\bullet}/Tyr_D$ spectra obtained in the presence of unlabeled and $^{13}C_1$(4)-labeled Tyr (Figure 2C, thin and bold lines): (i) the shift from 1250 to 1226 cm^{-1} of a negative signal characteristic of Tyr_D and (ii) the shift of a positive signal at 1503 to 1476 cm^{-1}. The positive band at 1503 cm^{-1} is thus assigned to unlabeled $Tyr_D^{\bullet}$. This band is strongly reduced in Figure 2C, bold line, while it seems only partially bleached in spectra of Figure 2A,B (bold line), where a broad positive mode appears at ≈1496 cm^{-1}. The same yield of incorporation is observed for $^{13}C_1$(4)-, $^{13}C_6$-, and $^{2}H_4$-Tyr. Thus we conclude that, in addition to the mode of $Tyr_D^{\bullet}$ at 1503 cm^{-1}, other side-chain modes from Tyr_D and/or $Tyr_D^{\bullet}$ are present at 1550−1450 cm^{-1}. These modes are affected by $^{13}C_6$ or $^{2}H_4$ labeling but only weakly modified upon $^{13}C_1$(4)-Tyr labeling.

In the $Tyr_D^{\bullet}/Tyr_D$ spectra, isotope-sensitive signals from Tyr_D and $Tyr_D^{\bullet}$ are superimposed upon signals of residues other than Tyr_D affected by the photooxidation of Tyr_D. The IR signals of the $Tyr_D^{\bullet}/Tyr_D$ spectrum, which are not affected by Tyr labeling, are canceled in double-difference spectra calculated between the $Tyr_D^{\bullet}/Tyr_D$ spectra with unlabeled

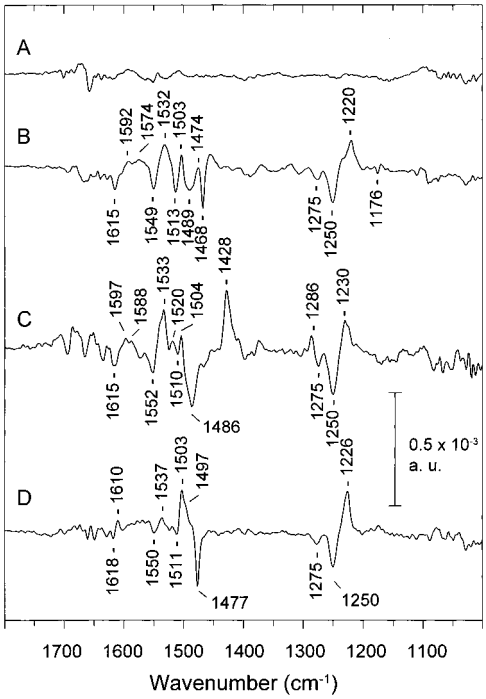

FIGURE 3: Difference spectra calculated from the $Tyr_D^{\bullet}/Tyr_D$ spectrum (thin line of Figure 2) minus (A) spectrum of Figure 1A obtained from WT PS II grown in normal BG-11 medium, (B) bold spectrum of Figure 2A, denoted ^{12}C minus $^{13}C_6$ spectrum, (C) bold spectrum of Figure 2B, denoted $^{1}H_4$ minus $^{2}H_4$, and (D) bold spectrum of Figure 2C, denoted ^{12}C minus $^{13}C_1$(4) spectrum. For reasons that are unclear, the noise level of spectrum C is higher in the 1700−1630-cm^{-1} region, as compared to spectra B and D. The intensities of spectra A−D are comparable since they were calculated from the same $Tyr_D^{\bullet}/Tyr_D$ reference spectrum recorded on cores isolated from *Synechocystis* grown in BG-11 medium supplemented with unlabeled aromatic amino acids (Figure 2, thin line).

minus labeled tyrosines. These double difference spectra are shown in Figure 3B−D for Tyr $^{13}C_6$, $^{2}H_4$, and $^{13}C_1$(4) labeling, respectively. The quality of the subtraction is determined by the size of residual signals in the 1730−1630-cm^{-1} region, where the most intense IR modes in the $Tyr_D^{\bullet}/Tyr_D$ spectra are present (Figure 1) but where no modes of Tyr side chain are expected to contribute (see below, *40*, *41*). Figure 3A shows the difference between $Tyr_D^{\bullet}/Tyr_D$ spectra obtained with *Synechocystis* sp. PCC 6803 grown in BG-11 medium supplemented with unlabeled aromatic amino acids minus those obtained with the cyanobacteria grown in normal BG-11 medium. The amplitude of the strongest signal of this spectrum, at ≈1650 cm^{-1} (Figure 3A), corresponds to less than 8% that of the largest signals of the $Tyr_D^{\bullet}/Tyr_D$ spectrum at 1653/1645 cm^{-1} (Figure 1). The absence of significant signals in spectrum A (Figure 3) shows the high reproducibility of the method and the confidence level for the interpretation of spectra in Figure 3B−D. Identification of the IR modes of Tyr_D and $Tyr_D^{\bullet}$ in spectra B to D is made by comparison with absorption spectra of unlabeled and labeled Tyr recorded in solution.

IR Spectra of Tyr in Solution. Spectra A−D in Figure 4 correspond to unlabeled, $^{13}C_6$-, $^{2}H_4$-, and $^{13}C_1$(4)- Tyr, in acidic (HCl) solutions at pH 2, respectively. Common signals in these spectra at 1734−1732, 1533, 1450−1441, and 1290 cm^{-1} are assigned to vibrations of the amino acid and β-methylene of Tyr (*40*), insensitive to isotope substitution of the phenol ring. For the protonated Tyr side chain,

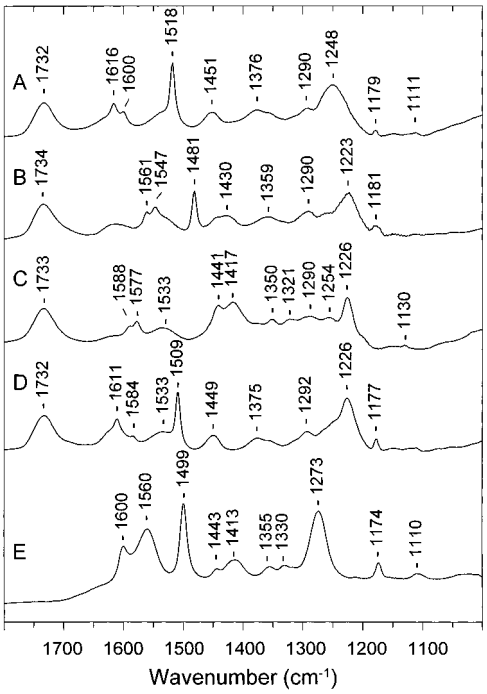

FIGURE 4: Absorption spectra of (A) Tyr in HCl, (B) $^{13}C_6$-Tyr, (C) $^2H_4$-Tyr, (D) $^{13}C_1(4)$-Tyr, and (E) Tyr in NaOH, after subtraction of a background spectrum arising from the absorption of the HCl or NaOH solution; 256 scans, 4 cm^{-1} resolution, 4 °C. Spectra are scaled to the same amplitude of the υ(CO) mode of terminal carboxylic acid at 1734−1732 cm^{-1}.

IR signals at 1616, 1600, 1518, 1248, and 1179 cm^{-1} are assigned to the ring CC stretching modes υ_{8a}(CC) and υ_{8b}-(CC), the ring CC stretching and CH bending mode υ_{19}(CC), the CO stretching mode $\upsilon_{7'a}$(CO), and the ring CH bending mode 9 (δCH), respectively [according to the notation for benzene (*42*) and *p*-disubstituted benzene (*43*−*46*); the normal modes of *p*-cresol are illustrated in ref *46*]. At 1248 cm^{-1}, the bending vibration of the tyrosine hydroxyl δ(COH) which gives a strong IR signal, is superimposed upon the $\upsilon_{7'a}$(CO) mode. The 9 (δCH) mode excepted, these vibrations are largely sensitive to $^{13}C_6$ labeling (Figure 4B) and appear for $^{13}C_6$-Tyr at 1561 (−55), 1547 (−53), 1481 (−37), and 1223 (−25) cm^{-1}. The frequency shifts induced by $^2H_4$-Tyr labeling are also large yet of different amplitudes (Figure 4C). Shifts by ≈−25 cm^{-1} are observed for the υ_{8a}(CC), υ_{8b}(CC), and $\upsilon_{7'a}$(CO) + δ(COH) modes, which appear at 1588, 1577, and 1226 cm^{-1}, respectively. The υ_{19}(CC) ring mode at 1518 cm^{-1} for Tyr is replaced by two bands at 1441 and 1417 cm^{-1} for $^2H_4$-Tyr, presumably due to Fermi resonance (*47*). The downshift of the υ_{19}(CC) mode of Tyr is estimated at ≈−90 cm^{-1} upon $^2H_4$ labeling, by comparison with *p*-cresol (*46*). Downshifts of smaller amplitudes are observed upon Tyr $^{13}C_1(4)$-labeling (−5 to −16 cm^{-1}) except for the mode at 1248 cm^{-1}, which is downshifted by 22 cm^{-1} to 1226 cm^{-1} (Figure 4D). This large shift is due to the involvement of vibrations at the C4−O bond of Tyr at 1248 cm^{-1}.

The Tyr side-chain modes are also sensitive to the protonation state of the phenol group (*40, 41, 48*). This is illustrated in Figure 4E, recorded with Tyr in NaOH solution at pH 13. The υ_{8a}(CC) and υ_{19}(CC) modes at 1616 and 1518 cm^{-1} and the $\upsilon_{7'a}$(CO) mode at ≈1248 cm^{-1} for Tyr in acidic solution appear at 1600, 1499, and 1273 cm^{-1}, respectively, for tyrosinate.

Effect of Tyr Labeling in PS II. In the double-difference spectra of Figure 3B−D, the isotope-sensitive modes of unlabeled Tyr_D give negative signals and those from unlabeled $Tyr_D^•$ positive ones. The corresponding modes of labeled Tyr_D appear as positive signals and those of labeled $Tyr_D^•$ give negative bands. Since the three labels affect differently the Tyr ring modes, common negative signals in Figure 3B−D most probably correspond to modes of unlabeled Tyr_D and common positive ones to unlabeled $Tyr_D^•$, while the specific bands of each spectrum are due to labeled Tyr_D and $Tyr_D^•$. Common negative bands in Figure 3B,C at 1615, 1513−1510, and 1250 cm^{-1} have frequencies close to those observed at 1616, 1518, and 1248 cm^{-1} in Figure 4A for Tyr in acidic solution and are assigned to modes of unlabeled Tyr_D. By analogy with Figure 4A, the negative band at 1615 cm^{-1} in Figure 3B,C is assigned to the υ_{8a}-(CC) mode of Tyr_D. The positive signals observed at ≈1574 cm^{-1} in Figure 3B and at 1588 cm^{-1} in Figure 3C could be the corresponding υ_{8a}(CC) mode of $^{13}C_6$- and $^2H_4$-Tyr_D, respectively, since the isotope-induced downshifts of −41 and −27 cm^{-1} are close to those observed for Tyr in solution (−55 and −28 cm^{-1}, Figure 4B,C; Table 1). The small differential signal negative at 1618 cm^{-1} and positive at 1610 cm^{-1} observed in Figure 3D in this region is also in agreement with the 5 cm^{-1} downshift observed on the υ_{8a}-(CC) Tyr mode in solution upon $^{13}C_1(4)$ labeling (Figure 4D). The signal at 1513−1510 cm^{-1} is assigned to the υ_{19}(CC) mode of unlabeled Tyr_D and specific signals of Figure 3B,C at 1474 and 1428 cm^{-1}, to the corresponding υ_{19}(CC) mode of $^{13}C_6$- and $^2H_4$-Tyr_D, respectively, since the amplitude of the shifts induced by the Tyr $^{13}C_6$- and $^2H_4$ labeling in PS II (−39 and −82 cm^{-1}) are comparable to those observed for the υ_{19}(CC) mode of Tyr *in vitro* (−37 and ≈−90 cm^{-1}, Table 1). The assignment of the signal at 1250 cm^{-1} to a mode of Tyr_D is already deduced from the spectra of Figure 2. The shifts by −30, −20, and −24 cm^{-1} observed upon $^{13}C_6$-, $^2H_4$-, and $^{13}C_1(4)$-Tyr labeling (Figure 3B−D) are similar to those observed for the $\upsilon_{7'a}$(CO) + δ(COH) mode of Tyr in acidic solution (Figure 4, Table 1). A second negative signal is observed in the absorption region of the $\upsilon_{7'a}$(CO) and δ(COH) modes at 1275 cm^{-1} in Figure 3B−D. This signal, revealed by the double difference spectra, can also be confidently assigned to unlabeled Tyr_D. The assignment of the signals at 1275 and 1250 cm^{-1} is detailed below. Finally, a negative mode is observed at 1552−1549 cm^{-1}, which is sensitive to the three different labels (Figure 3B−D). It is therefore tentatively attributed to the side chain of Tyr_D although there is no clear equivalent of this signal in the FTIR spectra of Tyr *in vitro.* The corresponding mode of $^2H_4$- and $^{13}C_1(4)$-Tyr_D could contribute at 1520 and 1537 cm^{-1}, respectively.

$^{13}C_1(4)$-Tyr labeling (Figures 2C and 3D) demonstrates that a positive signal at 1503 cm^{-1} is due to $Tyr_D^•$. Vibrations at the C4−O bond of Tyr are the most sensitive to $^{13}C_1(4)$-Tyr labeling (Figure 4D). Therefore, the signal at 1503 cm^{-1} is assigned to the υ(CO) mode of $Tyr_D^•$. The 1503-cm^{-1} band of $Tyr_D^•$ is also observed in the double difference spectra B (1504 cm^{-1}) and C of Figure 3. The corresponding mode of $^{13}C_6$- and $^2H_4$-$Tyr_D^•$ can be confidently assigned at 1468 and 1486 cm^{-1}, respectively. This represents downshifts by 35 and 18 cm^{-1} upon $^{13}C_6$ and $^2H_4$ labeling (Table 1). A large positive signal is present at 1533−1532 cm^{-1} in Figure 3B,C. Although no equivalent

Table 1: Tyrosine Side-Chain Modes Sensitive to the Isotopic Substitution[a]

(A) IR Modes of Tyr in Solution and Tyr_D in WT PS II

IR modes	Tyr-HCl	**Tyr_D**	$^{13}C_1$(4)-Tyr	**$^{13}C_1$(4)-Tyr_D**	$^{13}C_6$-Tyr	**$^{13}C_6$-Tyr_D**	$^2H_4$-Tyr	**$^2H_4$-Tyr_D**
ν_{8a}(CC)	1616	**1615**	1611 (−5)	**1610 (−5)**	1561 (−55)	**1574 (−41)**	1588 (−28)	**1588 (−27)**
ν_{8b}(CC)	1600		1584 (−16)		1547 (−54)		1577 (−24)	
		1552−1549		**1537 (−13)**		**1523 (−27)**		**1520 (−32)**
ν_{19}(CC)	1518	**1513−1510**	1509 (−9)	**1497 (−14)**	1481 (−37)	**1474 (−39)**	1417 (≈−101)	**1428 (−82)**
$\nu_{7'a}$(CO)	1248	**1275**						
δ(COH)	1248	**1250**	1226 (−22)	**1226 (−24)**	1223 (−25)	**1220 (−30)**	1226 (−22)	**1230 (−20)**
9δ(CH)	1179	***1175***	1177		1181			

(B) IR Modes of Tyr$^\bullet$ in Solution and $Tyr_D^\bullet$ in WT PS II

IR modes	Tyr•	**$Tyr_D^\bullet$**	$^{13}C_1$(4)-Tyr$^\bullet$	**$^{13}C_1$(4)-$Tyr_D^\bullet$**	$^{13}C_6$-Tyr$^\bullet$	**$^{13}C_6$-$Tyr_D^\bullet$**	$^2H_4$-Tyr$^\bullet$	**$^2H_4$-$Tyr_D^\bullet$**
ν(CC)		**1533−1532**				**1489 (−42)**		**1495 (−38)**
ν(CO)	1513	**1503**	1483 (−31)	**1477 (−26)**	1475 (−39)	**1468 (−35)**	1492 (−22)	**1486 (−18)**

(C) IR Modes of Tyr_D and $Tyr_D^\bullet$ in the D2-His189Gln Mutant

IR modes	**Tyr_D**	**$^2H_4$-Tyr_D**	IR modes	**$Tyr_D^\bullet$**	**$^2H_4$-$Tyr_D^\bullet$**
ν_{8a}(CC)	**1615**	**1592 (−23)**		**1533 vw**	
ν_{8b}(CC)	**1597**	**1574 (−23)**	ν (CO)	**1497**	**1479 (−18)**
ν_{19}(CC)	**1516**	**1407 (−109)**			
$\nu_{7'a}$(CO)	**1267**	**1228 (−39)**			
δ(COH)	**1228**				

[a] Numbers in parentheses indicate the shift induced by the labeling. vw, very weak.

signal is observed at ≈1533 cm^{-1} in Figure 3D, we tentatively assign the signal at 1532−1533 cm^{-1} in Figure 3B,C to a mode of unlabeled $Tyr_D^\bullet$ that is not altered by $^{13}C_1$(4) labeling. We propose that this mode is downshifted to ≈1489 cm^{-1} upon $^{13}C_6$ labeling and to ≈1495 cm^{-1} upon $^2H_4$ labeling (Figure 3B). Small positive signals at 1597−1592 cm^{-1} in Figure 3B,C appear at a frequency too high to account for a mode of $^{13}C_6$- or $^2H_4$-Tyr_D (Figure 4B,C). As positive signals come from either labeled Tyr_D or unlabeled $Tyr_D^\bullet$, the signals at 1597−1692 cm^{-1} may be due to unlabeled $Tyr_D^\bullet$. These signals are, however, at the detection limit of the method. The band assignment is summarized in Table 1.

His D2-189 Gln Mutant. Figure 5A shows the $Tyr_D^\bullet/Tyr_D$ FTIR difference spectra recorded on PS II of WT *Synechocystis* sp. PCC 6803 (thin line) and of the D2-His189Gln mutant (bold line). The mutation induces strong changes in the $Tyr_D^\bullet/Tyr_D$ spectrum. A new large positive signal appears at 1692 cm^{-1} and a negative one at 1659 cm^{-1} in Figure 5A (bold line). The negative band observed at 1624 cm^{-1} for WT PS II core particles (Figure 5A, thin line) is replaced by a positive band at 1623 cm^{-1} in the mutant (bold line). Two main IR contributions are expected for the side chain of Gln, the ν(C═O) mode at ≈1670 cm^{-1} and the ν(CN) + δ(NH) mode at ≈1610 cm^{-1} (*40*). The ν(C═O) mode is sensitive to interactions with the environment (data not shown; *47*, *49*) and has an absorption coefficient more than 5 times higher than those of the His side-chain modes, expected below 1630 cm^{-1} (*40*). Therefore, we propose that the signals at 1659 and 1692 cm^{-1} in spectrum 5A (bold line) correspond to the ν(C═O) mode of Gln, upshifted upon $Tyr_D^\bullet$ formation. The differential signals at 1652/1643/1634 cm^{-1} and also at 1702/1696 cm^{-1} seem not to be altered by the mutation, while the negative band at 1672 cm^{-1} in Figure 5A (thin line) is upshifted to 1677 cm^{-1} in the spectrum with bold line.

The IR modes of Tyr_D and $Tyr_D^\bullet$ are also largely modified in the D2-His189Gln mutant. In particular, there is no clear equivalent in Figure 5A (bold line) of the negative signal observed at 1250 cm^{-1} in Figure 5A (thin line) and assigned to Tyr_D in WT PS II. Two negative bands appear in this region at ≈1271 and 1228 cm^{-1} for the mutant (bold line). The positive signals of the $Tyr_D^\bullet/Tyr_D$ spectrum recorded with WT PS II at 1531 and 1503 cm^{-1}, sensitive to Tyr $^{13}C_6$ and $^2H_4$ labeling (Figure 3B,C), are also absent in the $Tyr_D^\bullet/Tyr_D$ spectrum recorded with the mutant, for which a positive band is observed at 1497 cm^{-1} (Figure 5A, bold line).

The IR modes of Tyr_D and $Tyr_D^\bullet$ are identified in the D2-His189Gln mutant by the comparison of $Tyr_D^\bullet/Tyr_D$ spectra recorded in the presence of unlabeled or $^2H_4$-labeled Tyr (Figure 5B, thin and bold lines, respectively). As already noticed for WT PS II (Figure 2), the two $Tyr_D^\bullet/Tyr_D$ spectra of Figure 5B are very similar above 1630 cm^{-1}. Negative signals at 1615, 1516, and 1271 cm^{-1} of Figure 5B (thin line) are absent in the $Tyr_D^\bullet/Tyr_D$ spectrum recorded with the mutant in the presence of $^2H_4$-Tyr, while new negative bands appear at 1592, 1407, and 1228 cm^{-1} (bold line). The positive band at 1497 cm^{-1} in Figure 5B (thin line) is downshifted to 1479 cm^{-1} (Figure 5B, bold line) upon $^2H_4$-Tyr labeling.

The $^1H_4$ minus $^2H_4$ double-difference spectrum obtained by subtraction of spectra in Figure 5B is shown in Figure 5C. Small negative bands at 1615 and 1597 cm^{-1} and positive ones at 1592 and 1574 cm^{-1} are assigned to the ν_{8a}(CC) and ν_{8b}(CC) modes of unlabeled and $^2H_4$-labeled Tyr_D, respectively, in the mutant. The frequencies and the downshifts by 23 cm^{-1} upon $^2H_4$ labeling are very similar to those observed for Tyr in solution (Figure 4A,C, Table 1). Similarly, comparison with *in vitro* data on Tyr (Figure 4A,C) show that the negative signal at 1516 cm^{-1} and positive one at 1407 cm^{-1} in Figure 5C are likely candidates for the ν_{19}(CC) mode of Tyr_D and $^2H_4$-Tyr_D, in the D2-His189Gln mutant. In the absorption region of the Tyr $\nu_{7'a}$-(CO) and δ(COH) modes, the $^1H_4$ minus $^2H_4$ difference spectrum reveals a negative band at 1267 cm^{-1} and a very small one at 1221 cm^{-1} (Figure 5C). These bands are assigned to IR modes of Tyr_D and will be discussed below. The positive band at 1228 cm^{-1} in Figure 5C is assigned to the mode of $^2H_4$-Tyr_D, corresponding to that at 1267 cm^{-1} of Tyr_D, downshifted by 39 cm^{-1}.

Spectra in Figure 5B,C show the downshift of a positive signal of $Tyr_D^\bullet$ from 1497 to 1479 cm^{-1} upon $^2H_4$ labeling.

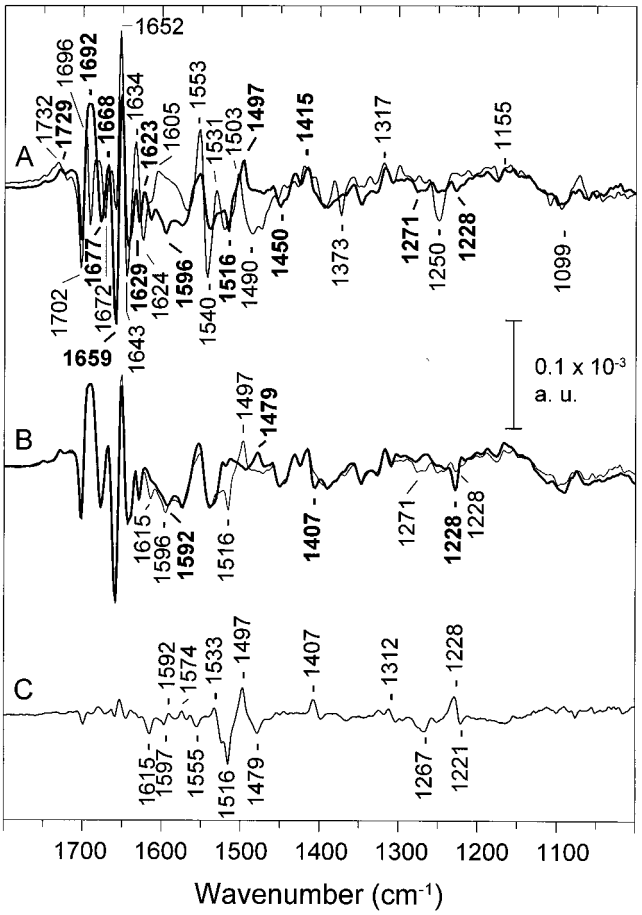

FIGURE 5: $Tyr_D^{\bullet}/Tyr_D$ FTIR difference spectra. (A) Thin line, recorded using PS II cores from WT PS II; bold line, recorded using cores from the D2-His189Gln mutant of *Synechocystis* sp. *PCC* 6803. (B) Thin line, $Tyr_D^{\bullet}/Tyr_D$ spectrum recorded on cores from the D2-His189Gln mutant of *Synechocystis* sp. *PCC* 6803 grown in the presence of unlabeled aromatic amino acids, 138 640 scans; bold line, grown in the presence of $^2H_4$-Tyr, 92 520 scans. (C) $^1H_4$ minus $^2H_4$ difference spectrum for the mutant calculated from spectra in (A); the scaling factor between the two spectra has been optimized to suppress the signals not influenced by the Tyr isotope labeling. Resolution 4 cm^{-1}, 4 °C.

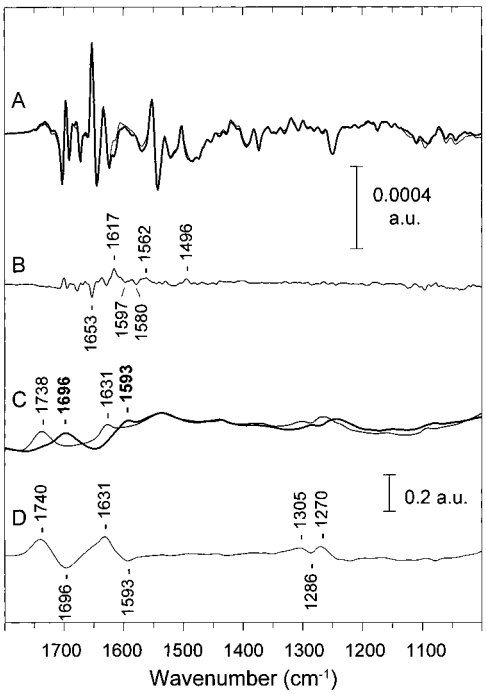

FIGURE 6: (A) $Tyr_D^{\bullet}/Tyr_D$ spectra recorded using PS II cores from the His-tolerant strain of *Synechocystis* sp. PCC 6803 grown in the presence of unlabeled His (thin line), 126 720 scans, and [U-^{13}C]-His (bold line), 138 960 scans; (B) ^{12}C minus [U-^{13}C]His difference spectrum; (C) absorption spectra of [U-^{12}C]His (thin line) and [U-^{13}C]His (bold line), 512 scans in HCl, after subtraction of the absorption from HCl; (D) [U-^{12}C]His minus [U-^{13}C]His difference spectrum calculated from spectra in (C); 4 cm^{-1} resolution.

The shift by -18 cm^{-1} is comparable to that observed for the band at 1503 cm^{-1} assigned to the ν(CO) mode of $Tyr_D^{\bullet}$ in WT PS II (Figure 2). Therefore, the signal at 1497 cm^{-1} in Figure 5B (thin line) is assigned to the ν(CO) mode of $Tyr_D^{\bullet}$ in the D2-His189Gln mutant. A positive band is also revealed at 1533 cm^{-1} in the $^1H_4$ minus $^2H_4$ spectrum of Figure 5C, but with a much smaller amplitude than that observed at this frequency in WT PS II, and tentatively assigned to $Tyr_D^{\bullet}$ (Figure 3D).

Histidine ^{13}C Labeling. The large perturbation of the vibrations at the C4−O bond of Tyr_D and $Tyr_D^{\bullet}$ upon His D2-189 replacement by Gln points to a specific interaction between D2-His189 and the hydroxyl group of Tyr_D in WT PS II (*3, 17, 20*−*23*). Also, it has been proposed that D2-His189 could be the base proton acceptor upon $Tyr_D^{\bullet}$ formation (*3, 17, 21, 22*). To test this hypothesis, we attempted to identify the contribution from IR modes of histidine in the $Tyr_D^{\bullet}/Tyr_D$ spectrum. Therefore, $Tyr_D^{\bullet}/Tyr_D$ spectra recorded on PS II cores from a histidine-tolerant strain of *Synechocystis* sp. PCC 6803 grown in the presence of unlabeled histidine or of [U-^{13}C]histidine are compared in Figure 6A (thin and bold line, respectively). The [U-^{13}C]-His labeling should affect all the vibrational modes of histidine, both from the side chain, expected below 1630 cm^{-1}, and from the peptide carbonyl, expected between 1620 and 1690 cm^{-1}. The only significant difference between the two $Tyr_D^{\bullet}/Tyr_D$ spectra displayed in Figure 6A is observed at 1620−1615 cm^{-1}, where the signal is more negative in the spectrum recorded in the presence of [U-^{13}C]His (bold line). The ^{12}C-His minus [U-^{13}C]His double-difference spectrum is presented in Figure 6B. The small size of signals in Figure 6B is not due to partial incorporation of the labeled histidine, which is estimated at ≈85% for histidine with ^{15}N-labeled side chain (*36*). A more likely explanation is the weak absorption coefficients (ϵ) of the His side-chain modes, as compared for example to those of Tyr *in vitro* (*40*). Figure 6C shows the FTIR absorption spectra of unlabeled histidine (thin line) and [U-^{13}C]histidine (bold line) in HCl solution. The largest mode of protonated histidine ($HisH_2^+$) *in vitro* is the ν(C═C) imidazole ring mode at 1631 cm^{-1} shifting by -38 cm^{-1} to 1593 cm^{-1} upon U-^{13}C labeling (Figure 6C). In the difference spectrum $HisH_2^+$ minus [U-^{13}C]$HisH_2^+$ of Figure 6D, the ν(C═C) mode is the only side-chain mode of $HisH_2^+$ that is observed beyond the IR modes of the His amino acid function (at 1740/1696 cm^{-1} and 1305/1286/1270 cm^{-1}). By reference to data in Venyaminov and Kalnin (*40*), the ϵ of the $HisH_2^+$ ν(C═C) mode at 1631 cm^{-1} is estimated at 250 ± 20 $L{\cdot}mol^{-1}{\cdot}cm^{-1}$. For histidine with a neutral imidazole side chain (HisH), two signals are expected at ≈1595 and/or ≈1575 cm^{-1} for the ν(C═C) mode (*50*). The ϵ of the ν(C═C) mode of HisH at 1595 cm^{-1} is reported at 70 ± 10 $L{\cdot}mol^{-1}{\cdot}cm^{-1}$ (*40*), i.e., 3.5 times smaller than that of $HisH_2^+$ and 6 times smaller than that of the Tyr ring υ_{19}-(CC) mode at 1518 cm^{-1}. From these data, we can conclude

that it will be very difficult to detect IR modes of HisH in the double-difference spectrum of Figure 6B but that the υ(C═C) mode of $HisH_2^+$ could be detected. The largest band in Figure 6B is a positive band at 1617 cm^{-1}. Small negative bands at 1597 and 1580 cm^{-1} and a positive one at 1496 cm^{-1} are also reproducibly observed with different pairs of unlabeled and [U-^{13}C]His PS II samples. The positive band at 1617 cm^{-1} and negative one at 1580 cm^{-1}, in Figure 6B, could correspond to the υ(C═C) mode of $HisH_2^+$ and [U-^{13}C]-$HisH_2^+$, respectively, in the $Tyr_D^\bullet$ state. The relative band intensities and the shift by −37 cm^{-1} upon [U-^{13}C]His labeling correspond to that observed for this mode in solution (Figure 6C,D). The 14 cm^{-1} downshift of the υ(C═C) mode of $HisH_2^+$ at 1617 cm^{-1} *in situ* as compared to data *in vitro* (Figure 7C) could be due to strong hydrogen bonding of the imidazole protons in PS II. The assignment of the positive signal at 1617 cm^{-1} in Figure 6B to the υ(C═C) mode of $HisH_2^+$, remains tentative, and contribution at this frequency of the stretching mode of the [U-^{13}C]His peptide carbonyl cannot be excluded.

DISCUSSION

Combination of FTIR difference spectroscopy and specific tyrosine ^{2}H- and ^{13}C-labeling in *Synechocystis* sp. PCC 6803 was previously used to identify the IR modes of Tyr_D and Tyr_Z in PS II (*51*). In particular, the υ(CO) mode of $Tyr_D^\bullet$ was tentatively assigned at 1473 cm^{-1} and a signal at 1533 cm^{-1} was proposed to account for Tyr_D on the basis of changes in IR signal intensities. The corresponding modes for labeled Tyr_D and $Tyr_D^\bullet$ were not identified. The spectra by MacDonald et al. (*51*) are very different from those reported in the present study. We have previously discussed in detail the probable reasons for the strong differences between the two sets of spectra (*32*). In light of the present results and those of Hienerwadel et al. (*32*), we disagree with the assignments of the IR υ(CO) modes of $Tyr_D^\bullet$ and $Tyr_Z^\bullet$ at 1473 and 1477 cm^{-1} proposed by MacDonald et al. (*51*) and Bernard et al. (*52*) and attribute them to some mixing of PS II donor- and acceptor-side IR difference signals. This mixing is still present in more recent work (*53*, *54*). The results described in the present paper show that the study of pure $Tyr_D^\bullet/Tyr_D$ FTIR difference spectra using samples with specifically labeled Tyr, together with the comparison with model spectra obtained *in vitro*, allows the identification of the majority of the side chain modes of Tyr_D and $Tyr_D^\bullet$ in both WT and D2-His189Gln mutant PS II.

IR Modes of Tyr_D. In WT PS II, five IR signals are identified as side-chain modes of Tyr_D. Signals at 1615 and 1513−1510 cm^{-1} are confidently assigned to the υ_{8a}(CC) and υ_{19}(CC) ring modes of Tyr_D, respectively. The frequency of these modes is sensitive to the protonation state of Tyr and appear at 1600 and 1499 cm^{-1} for tyrosinate (Figure 4A,E, *41*). For the related model compound of Tyr side chain, *p*-cresol, it was shown that the frequency of these modes is not sensitive to the environment (*46*, *55*, *56*). Thus, the frequencies at 1615 and 1513−1511 cm^{-1} for Tyr_D *in situ* show without ambiguity that Tyr_D is protonated in PS II at pH 6.

Two isotope-sensitive signals are identified at 1275 and 1250 cm^{-1} for Tyr_D in the absorption region of the $\upsilon_{7'a}$(CO) and δ(COH) modes. Both signals are modified upon

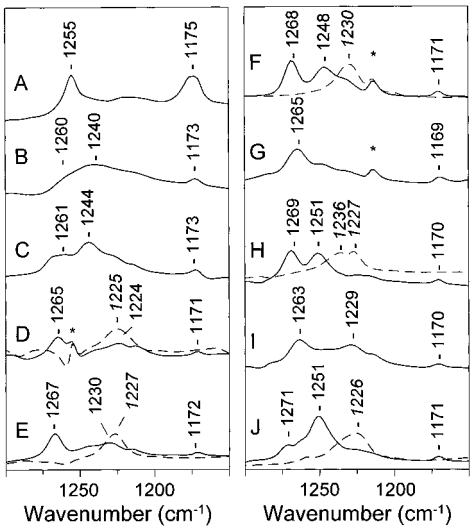

FIGURE 7: Effect of hydrogen bonding on the IR modes of *p*-cresol. Continuous-line: spectra of *p*-cresol in (A) CCl_4, (B) water, (C) 2-propanol, (D) 1,4-dioxan, (E) *N*,*N*′-dimethylformamide, (F) pyridine, (G) *p*-cresol-OD in pyridine [the yield of *p*-cresol deuteration was estimated from the intensity of the ν(OH) and ν-(OD) IR modes to 75%], (H) 1-MeIm, (I) $1MeImH^+$, obtained by acidification of 1-MeIm with gazeous HCl, and (J) 4-MeImH are shown. 128 scans. Spectra with dashed lines represent the IR absorption of $^2H_4$-*p*-cresol in the same solvents. Spectra are shown after subtraction of the IR absorption of the solvent; remaining peaks from the solvent are marked by asterisks. Cresol concentration 200 mM, 4 cm^{-1} resolution, 298 K.

$^{13}C_1$(4)-Tyr labeling, showing that both involve vibration at the C4−O bond (Figure 3D). Although the signal at 1275 cm^{-1} appears at a frequency close to that observed for tyrosinate at pH 12 (1273 cm^{-1}, Figure 4E), the presence of a population of deprotonated Tyr_D in PS II at pH 6 is ruled out since no signals characteristic of tyrosinate, at ≈1600 and ≈1499 cm^{-1}, can be assigned to unlabeled Tyr_D in Figure 3B−D. The origin of the two bands observed at 1275 and 1250 cm^{-1} for Tyr_D in PS II is discussed by comparison with IR absorption spectra of *p*-cresol in solvents providing different interactions with the phenolic hydroxyl group (Figure 7).

The $\upsilon_{7'a}$(CO) and δ(COH) IR modes absorb strongly in the 1300−1100-cm^{-1} region. These modes appear at 1255 and 1175 cm^{-1} for *p*-cresol in the apolar and aprotic solvent CCl_4 (Figure 7A), i.e., for *p*-cresol free from hydrogen-bond interactions (*45*, *46*). They give rise to a broad band at 1260−1240 cm^{-1} for *p*-cresol in H_2O (Figure 7B). Two distinct bands with different frequencies and amplitudes are observed for *p*-cresol in solvents providing different kinds of hydrogen-bonding interactions (Figure 7C−F and H−J; *55*, *57*−*59*). In pyridine, two signals of similar amplitude appear at 1268 and 1248 cm^{-1} (Figure 7F). Two bands are also observed at 1272 and 1245 cm^{-1} for phenol in a mixture of phenol/pyridine/propionitrile at a molar ratio of 1:10:16 (not shown), conditions in which $(phenol)_1(pyridine)_1$ complexes are formed (*60*). Thus the two bands observed at 1268 and 1248 cm^{-1} for *p*-cresol in pyridine (Figure 7E) are not due to inhomogeneity of $(cresol)_n-(pyridine)_m$ interactions but represent two modes of *p*-cresol. These modes are affected differently upon deuteration of the *p*-cresol hydroxyl (Figure 7G). The signal at 1268 cm^{-1} is downshifted by 3 cm^{-1} and thus assigned to the $\upsilon_{7'a}$(CO) mode of *p*-cresol, while the well-defined band at 1248 cm^{-1} is

Table 2: IR Modes of *p*-Cresol and $^2H_4$-*p*-Cresol in Different Solvents[a]

solvent		υ_{8a}(CC)	υ_{8b}(CC)	υ_{19}(CC)	$\upsilon_{7'a}$(CO)	δ(COH)	9δ(CH)	δ(CH)
CCl_4	*p*-cresol	1618	1598	1515	1255	1175		1103
water	*p*-cresol	1618	1601	1516	1260−1240	1260−1240	1173	1105
2-propanol	*p*-cresol	1617	1599	1516	1261	1244	1172	1103
	$^2H_4$-p-cresol	*1593*	*1579*	*1442*	*1225*		*1127*	
dioxane	*p*-cresol	1617	1597	1516	1265	1224	1172	1102
	$^2H_4$-p-cresol	*1600*	*1587*	*1441*	*1225*			
N,*N*′-DMF	*p*-cresol	1619	1596	1516	1267	1230	1171	1106
	$^2H_4$-p-cresol	*1588*	*1576*	*1439*	*1227*		*1126*	
pyridine	*p*-cresol	1615		1515	1268	1246	1170	1104
	$^2H_4$-p-cresol		*1575*	*1442*	*1230*		*1126*	
	***p*-cresol-OD**	**1612**		**1513**	**1265**		**1169**	**1105**
4-MeImH	*p*-cresol	1614	1598	1515	1271	1251	1171	1107
	$^2H_4$-p-cresol		*1578*	*1426*	*1226*		*1125*	
1-MeIm	p-cresol	1613	1595	1514	1269	1251	1170	1104
	$^2H_4$-p-cresol	*1585*	*1575*	*1439*	*1230*		*1127*	
1-MeImH$^+$	*p*-cresol	1614	1597	1515	1263	1229	1170	1105
	$^2H_4$-p-cresol	*1591*	*1573*	*1442*	*1224*		*1125*	
TCl-acetic	*p*-cresol	1613	1601	1514	1235		1173	1105

[a] The IR frequencies for $^2H_4$-*p*-cresol are given in italic type. The IR frequencies for *p*-cresol with deuteroxyl in pyridine are given in boldface type.

strongly reduced and therefore assigned to the *p*-cresol δ-(COH) mode. These experiments confirm literature data on the IR modes of *p*-cresol in pyridine (*55, 59*). By analogy with signals observed for *p*-cresol in pyridine, the signals at 1271−1261 cm^{-1} and at 1251−1224 cm^{-1} in Figure 7C−J are assigned to the $\upsilon_{7'a}$(CO) and δ(COH) modes of *p*-cresol, respectively.

The frequency of the $\upsilon_{7'a}$(CO) mode is observed at 1271−1265 cm^{-1} for *p*-cresol complexes with various hydrogen acceptors in panels D−F, H, and J of Figure 7 (see also *55*−*59*). Dioxane, *N*,*N*′-dimethylformamide (DMF), and pyridine have increasing hydrogen acceptor capacity, as measured by the enthalpy of hydrogen-bond formation with *p*-fluorophenol (*61*). A frequency upshift of the $\upsilon_{7'a}$(CO) IR mode is observed upon increase of the hydrogen acceptor character of the solvent molecule (Figure 7D−F, Table 2). The highest frequency is observed for *p*-cresol in interaction with 4-MeImH. In protonated 1-methylimidazole (1-MeImH$^+$), where the interaction is formed between the NH proton of 1-MeImH$^+$ and the oxygen of *p*-cresol, the $\upsilon_{7'a}$(CO) mode of *p*-cresol is downshifted by 6 cm^{-1} (Figure 7I). Lower frequencies are also observed for the $\upsilon_{7'a}$(CO) mode of *p*-cresol in the hydrogen-bond donor and acceptor 2-propanol (Figure 7C), and for *p*-cresol free from interactions (Figure 7A; *45, 46)*. This study further defines the relationships reported previously by RR spectroscopy between the frequency of the $\upsilon_{7'a}$(CO) of *p*-cresol and Tyr and the proton acceptor character of the solvent (*56*). The frequency and intensity of the δ(COH) IR mode also seem sensitive to the nature of the group interacting with the *p*-cresol hydroxyl. It appears as a strong band at 1248−1251 cm^{-1} for *p*-cresol hydrogen-bonded to the ring nitrogen of pyridine, 1-MeIm or 4-MeImH (Figure 7F,H,I), while it gives a band of small amplitude at lower frequencies (1224−1230 cm^{-1}) for *p*-cresol hydrogen-bonded to the ring oxygen of dioxane or to the amide carbonyl of DMF (Figure 7D,E). This correlation is strengthened by the frequencies at 1230−1229 cm^{-1} reported in the literature for the δ(COH) mode of *p*-cresol hydrogen-bonded to the C═O group of tetramethylurea or dimethylamine (*57, 58*) and at 1240−1246 cm^{-1} for *p*-cresol in interaction with pyridine (*55, 59*). Thus both the δ(COH) and $\upsilon_{7'a}$(CO) IR modes can be used to discriminate the different kinds of interactions formed by a Tyr side chain with its environment in a protein.

By analogy with results obtained with *p*-cresol (Figure 7), the two modes observed at 1275 and 1250 cm^{-1} for Tyr_D in PS II, are assigned to the $\upsilon_{7'a}$(CO) and δ(COH) modes of Tyr_D respectively. For Tyr_D in WT PS II, the presence of the two bands, their frequency at 1275 and 1250 cm^{-1}, and the large size of the band at 1250 cm^{-1} indicate the presence of a hydrogen bond between the hydroxyl group of Tyr_D and the unprotonated nitrogen of a histidine side chain. We can rule out the possibility of a hydrogen bond to an amide carbonyl or to a water molecule. These observations strongly support the hypothesis of a hydrogen-bond interaction between Tyr_D and the side chain of D2-His189. In ref *32*, we proposed that the υ(CO) mode of Tyr_D in spinach absorbs at 1252 cm^{-1}. The present detailed study on *Synechocystis* sp. PCC 6803 suggests that this signal corresponds to the δ(COH) mode of Tyr_D, and that the same interactions exist in spinach as in *Synechocystis* sp. PCC 6803 for the Tyr_D hydroxyl group.

IR Modes of $Tyr_D^\bullet$. Two signals are observed for $Tyr_D^\bullet$ at 1533−1532 and at 1503 cm^{-1}. The signal at 1503 cm^{-1} is largely sensitive to ^{13}C labeling at the C4 carbon of the C−O bond and is therefore assigned to the υ(CO) mode of $Tyr_D^\bullet$. The shift of −26 cm^{-1} is consistent with a calculated shift of −35 cm^{-1} in a simplified harmonic oscillator model for a pure CO mode absorbing at 1503 cm^{-1}. We have previously reported IR data on the phenoxyl radical of *p*-cresol (*32*), phenol, *p*-ethylphenol, and tyrosine (*62*) obtained by UV irradiation at 10 K. The largest IR signal is observed at 1513 cm^{-1} for the radicals of *p*-ethylphenol and tyrosine, and at 1503 cm^{-1} for the phenoxyl radical. In UV-induced FTIR difference spectra obtained with dilute solutions of unlabeled and $^{13}C_1$(4)-, $^{13}C_6$-, and $^2H_4$-labeled Tyr and of ^{18}O-*p*-cresol, this IR mode is downshifted by 31, 39, and 22 cm^{-1} for Tyr$^\bullet$, and by 16 cm^{-1} for ^{18}O-cresol$^\bullet$ (Table 1; Berthomieu, Boullais, and Boussac, manuscript in preparation). The large shift observed upon $^{13}C_1$(4)-Tyr$^\bullet$ labeling in solution and the fact that the 1503-cm^{-1} band of *p*-cresol$^\bullet$ is the only one affected by ^{18}O labeling confirm the assignment of the 1513−1503-cm^{-1} IR band to the υ(CO) mode of the radicals in solution. The shifts by −26, −35,

and −17 cm^{-1} identified for the 1503-cm^{-1} mode of $Tyr_D^•$ upon $^{13}C_1$(4), $^{13}C_6$, and $^2H_4$ labeling (Figure 3, Table 1) are slightly smaller but consistent with those observed for Tyr• in solution. This definitely allows the assignment of the 1503-cm^{-1} band of the $Tyr_D^•/Tyr_D$ FTIR difference spectra to the ν(CO) mode of $Tyr_D^•$ in WT PS II of *Synechocystis* sp. PCC 6803. The differences in frequency and in the shifts induced by isotope labeling reflect different interactions of the Tyr• in PS II and in solution.

These results are also strongly supported by data of the literature on the RR spectroscopy of phenoxyl radicals. A mode is observed by RR at 1502−1505 cm^{-1} for the phenoxyl radicals and at 1510 cm^{-1} for Tyr• (*63*−*66*). A recent study by Mukerjhee et al. (*67*) showed that this mode is shifted by −13 and −36 cm^{-1} upon ^{17}O and $^{13}C_6$ labeling; this was the first experimental evidence for its assignment to the ν(CO) mode of phenoxyl. The IR mode observed at 1503−1515 cm^{-1} that shifts by −16 cm^{-1} upon ^{18}O labeling clearly corresponds to the mode reported by RR.

A second mode is reported by RR at 1557−1550 cm^{-1} for the phenoxyl radical and at 1565 cm^{-1} for Tyr• (*63*−*67*). This mode is not sensitive to ^{17}O labeling but is downshifted by 45 cm^{-1} upon phenol $^{13}C_6$ labeling and by 44 cm^{-1} upon phenol $^2H_5$ labeling (*67*). The detection of IR side-chain modes of UV-induced Tyr• in this frequency range is prevented by the absorption of the amino acid group (*62*). The signal observed at 1532 ± 1 cm^{-1} in the ^{12}C minus $^{13}C_6$ and $^1H_4$ minus $^2H_4$ double-difference spectra of Figure 3B,C and assigned to $Tyr_D^•$ could correspond to the mode detected by RR spectroscopy at 1565 cm^{-1} (*67*).

Effect of D2-His189Gln Mutation on the IR Modes of Tyr_D and TyrD•. Five isotope-sensitive modes are also identified for the Tyr_D side chain in the D2-His189Gln mutant. The ν_{8a}(CC) and ν_{19}(CC) modes at 1615 and 1516 cm^{-1} have frequencies only slightly different from those observed for Tyr_D in WT PS II. They indicate that Tyr_D is also protonated in the D2-His189Gln mutant. In the mutant, the identification of the ν_{8b}(CC) mode of Tyr_D at 1597 cm^{-1} and the amplitude of the ν_{19}(CC) mode at 1516 cm^{-1} are closer to the IR spectrum of Tyr *in vitro* than those of Tyr_D in WT PS II, for which only the ν_{8a}(CC) mode is observed. The largest change induced by the mutation concerns the 1270−1200 cm^{-1} region, where two small bands appear at 1267 and ≈1228 cm^{-1} for the mutant. By comparison with data obtained with *p*-cresol in different solvents (Figure 7), the signals at 1267 and 1228 cm^{-1} are assigned to the $\nu_{7'a}$(CO) and δ(COH) modes of Tyr_D, respectively. Moreover, the relative intensities of the signals at 1267 and 1228 cm^{-1} show a strong analogy to the spectra observed for *p*-cresol in dioxane or DMF, which differ significantly from the spectra reported for *p*-cresol in pyridine, 1-MeIm, or 4-MeImH (Figure 7, Table 2). These frequencies are also close to those reported at 1269 and 1229 cm^{-1} for *p*-cresol interacting with tetramethylurea (*58*). These analogies argue strongly that Tyr_D is hydrogen-bonded in the D2-His189Gln mutant to the carbonyl group of Gln D2-189 side chain.

ENDOR (*14*, *16*, *17*, *23*) and ESEEM (*15*) spectroscopies have shown that $Tyr_D^•$ is hydrogen-bonded in WT PS II. Pulsed ENDOR using specific ^{15}N-isotope labeling (*23*) has shown that the source of hydrogen bond is the τ-nitrogen of D2-His189. This hydrogen bond is lost in the *Synechocystis* sp. PCC 6803 D2-His189Gln mutant (*17*, *22*, *23*). Ribonucleotide reductase, according to the three-dimensional structure (*68*) and ENDOR spectroscopy (*69*), contains a tyrosyl radical that is not hydrogen-bonded. It was shown by high-field EPR that the $Tyr_D^•$ in the D2-His189Gln mutant is very similar to that observed for ribonucleotide reductase, i.e., not hydrogen-bonded (*20*, *70*), while $Tyr_D^•$ of WT PS II is intermediate between the situation in the mutant and in a radical formed with Tyr *in vitro* (*70*, *71*).

Ribonucleotide reductase has been studied by RR spectroscopy and a mode at 1498 cm^{-1} has been assigned to the Tyr• of the catalytic cycle (*72*). We assign the ν(CO) mode of $Tyr_D^•$ at 1497 cm^{-1} in the D2-His189Gln mutant. This frequency is very close to that observed for ribonucleotide reductase, and this is an additional indication that $Tyr_D^•$ is not hydrogen-bonded in this mutant. In WT PS II, we assign the ν(CO) mode of $Tyr_D^•$ at 1503 cm^{-1} and for Tyr• formed by UV irradiation *in vitro*, this mode is assigned at 1513−1510 cm^{-1} (*62*, *64*). In solution, hydrogen bonds exist between water or another amino acid molecule and the phenolic oxygen of Tyr• (*62*). Therefore, the present study shows that hydrogen-bonding causes a frequency increase of the ν(CO) IR mode of Tyr•. For pure ν(C-O) or ν(C═O) stretching modes, hydrogen-bonding induces a downshift of the vibration frequency *(47)*, explained by a reduction in bond strength. For Tyr•, the strength of the C4−O bond is determined by electrons partially delocalized on the aromatic ring. The "ν(CO)" mode is not the pure stretching mode of an isolated CO group. It is coupled with vibrations, notably at the ring C3 and C5 carbons. This is illustrated, for example, in the normal mode calculations of Qin and Wheeler *(73, 74)*. Recently, the density-functional method has been used to calculate the effect of hydrogen bonding on the IR modes of PhO• and an upshift by 24 cm^{-1} is obtained for the PhO• ν(CO) mode upon hydrogen-bonding to two water molecules (Patrick O'Malley, personal communication).

As observed by high-field EPR (*20*), the IR data presented here show that the hydrogen bond to $Tyr_D^•$ in WT PS II is weaker than that observed for Tyr• in solution. It cannot be excluded, however, that other parameters than the formation of a hydrogen bond (e.g., charge distribution) also influence the frequency of the ν(CO) IR mode of the Tyr• radicals.

The other difference between the IR modes of $Tyr_D^•$ in WT PS II and in the D2-His189Gln mutant is the very small amplitude in the mutant of the signal at 1532 ± 1 cm^{-1} tentatively assigned to $Tyr_D^•$ in WT PS II. This signal was not detected for Tyr• radicals obtained by UV irradiation *in vitro*. It may be enhanced in WT PS II by electronic coupling between $Tyr_D^•$ and the imidazole ring of D2-His189.

This study also reveals that several IR difference signals in the $Tyr_D^•/Tyr_D$ spectrum are contributed by other protein modes. Common features in the $Tyr_D^•/Tyr_D$ spectra obtained with WT and D2-His189Gln mutant are the difference signals at 1702/1696 and 1653/1645 cm^{-1}. These signals are also observed in the $Tyr_D^•/Tyr_D$ spectrum recorded with PS II from spinach (Figure 1). The signals at 1653/1643 cm^{-1} may correspond to changes in peptide carbonyl group(s) within the α-helix carrying Tyr_D (*21*, *75*) or at Tyr_D itself (*62*). We proposed in Hienerwadel et al. (*32*) that the difference signal at 1702/1696 cm^{-1} could correspond to a vibration of the 9-keto ν(C═O) mode of a chlorophyll of P_{680}, since an electrochromic shift was observed upon $Tyr_D^•$ formation, which has been assigned to P_{680} (*38*). Preliminary

P_{680}^{+}/P_{680} FTIR spectra show that the stretching mode of the 9-keto group of one chlorophyll of P_{680} absorbs at 1700 cm^{-1} (*76*). A similar correlation between the electrochromic shift observed for the bacteriopheophytin upon Q_A reduction in the bacterial reaction center of *Rhodobacter sphaeroides* and changes in the frequencies of its vibrational modes has been recently shown by Breton et al. *(77).* However, contribution at 1702/1696 cm^{-1} of a peptide carbonyl cannot be excluded at present.

The $\upsilon_{7'a}$(CO) and δ(COH) modes of Tyr_D indicate that Tyr_D is hydrogen-bonded to the neutral imidazole side chain of histidine. The identification of a signal at 1617 cm^{-1} in the $Tyr_D^{\bullet}/Tyr_D$ spectrum upon His U-^{13}C labeling is compatible with the protonation of a His side chain upon $Tyr_D^{\bullet}$ formation in WT PS II. However, the small amplitude of the IR signals of His revealed by specific His U-^{13}C labeling in the $Tyr_D^{\bullet}/Tyr_D$ spectrum (Figure 6A) does not show clearly that His becomes protonated in all PS II centers upon $Tyr_D^{\bullet}$ formation. The presence of positive signals at 1725−1735 cm^{-1} in the $Tyr_D^{\bullet}/Tyr_D$ spectrum obtained with WT PS II could be due to the protonation of aspartic or glutamic side chain(s) upon $Tyr_D^{\bullet}$ formation. Positive signals are also observed at 1710−1729 cm^{-1} in the D2-His189Gln mutant. Additional studies are planned to investigate further the origin of these signals.

ACKNOWLEDGMENT

We gratefully acknowledge the excellent assistance of Ms. Mary-Jane Reeve for the preparation of many of the PS II core complexes of *Synechocystis* sp. PCC 6803. A. Menez and N. Gilles are acknowledged for providing part of the [U-^{13}C]His.

REFERENCES

1. Barry, B. A., and Babcock, G. T. (1987) *Proc. Natl. Acad. Sci. U.S.A. 84*, 7099−7103.
2. Barry, B. A., El Deeb, M. K., Sandusky, P. O., and Babcock, G. T. (1990) *J. Biol. Chem. 265*, 20139−20143.
3. Debus, R. J., Barry, B. A., Babcock, G. T., and MacIntosh, L. (1988) *Proc. Natl. Acad. Sci. U.S.A. 85*, 427−430.
4. Vermaas, W. F. J., Rutherford, A. W., and Hansson, O. (1988) *Proc. Natl. Acad. Sci. U.S.A. 85*, 8477−8481.
5. Debus, R. J., Barry, B. A., Sithole, I., Babcock, G. T., and MacIntosh, L. (1988) *Biochemistry 27*, 9071−9074.
6. Metz, J. G., Nixon, P. J., Rögner, M., Brudwig, G. W., and Diner, B. A. (1989) *Biochemistry 28*, 6960−6969.
7. Diner, B. A, and Babcock, G. T. (1996) in *Structure, Dynamics, and Energy Conversion Efficiency in Photosystem II, in Oxygenic Photosynthesis: the Light Reactions* (Ort, D., and Yocum, C., Eds.) Advances in Photosynthesis, Vol. 4, pp 213−247, Kluwer Academic Publishers, Dordrecht, The Netherlands.
8. Boussac, A., and Etienne, A.-L. (1984) *Biochim. Biophys. Acta 766*, 576−581.
9. Vass, I., and Styring, S. (1991) *Biochemistry 30*, 830−839.
10. Hoganson, C. W., and Babcock, G. T. (1994) in *Metal Ions in Biological Systems* (Sigel, H., and Sigel, A., Eds.) Vol. 30, pp 77−107, Marcel Dekker, New York.
11. Gilchrist, M. L., Ball, J. A., Randall, D. W., and Britt, R. D. (1995) *Proc. Natl. Acad. Sci. U.S.A. 92*, 9545−9549.
12. Hoganson, C. W., Lydakis-Simantiris, N., Tang, X. -S., Tommos, C., Warncke, K., Babcock, G. T., Diner, B. A., MaCracken, J., and Styring, S. (1995) *Photosynth. Res. 46*, 177−184.
13. Tommos, C., Tang, X.-S., Warncke, K., Hoganson, C. W., Styring, S., McCracken, J., Diner, B. A., and Babcock, G. T. (1996) *J. Am. Chem. Soc. 117*, 10325−10335.
14. Rodriguez, I. D., Chandrashekar, T. K., and Babcock, G. T. (1987) in *Progress in Photosynthesis Research* (Biggins, J., Ed.) pp 471−474, Martinus Nijhoff, Dordrecht, The Netherlands.
15. Evelo, R. G., Hoff, A. J., Dikanov, S. A., and Tyrishkin, A. M. (1989) *Chem. Phys. Lett. 161*, 479−484.
16. Mino, H., Satoh, J.-I., Kawamori, A., Toriyama, K., and Zimmerman, J.-L. (1993) *Biochim. Biophys. Acta 1144*, 426−433.
17. Tang, X.-S., Chisholm, D. A., Dismukes, G. C., Brudwig, G. W., and Diner, B. A. (1993) *Biochemistry 32*, 13742−13748.
18. Force, D. A., Randall, D. W., Britt, R. D., Tang, X.-S., and Diner, B. (1995) *J. Am. Chem. Soc. 117*, 12643−12644.
19. Tang, X.-S., Zheng, M., Chisholm, D. A., Dismukes, G. C., and Diner, B. (1996) *Biochemistry 35*, 1475−1484.
20. Un, S., Tang, X.-S., and Diner, B. A. (1996) *Biochemistry 35*, 679−684.
21. Svensson, B., Vass I., Cedergren, E., and Styring, S. (1990) *EMBO J. 7*, 2051−2059.
22. Tommos, C., Davidson, L., Svensson, B., Madsen, C., Vermaas, W. F. J., and Styring, S. (1993) *Biochemistry 32*, 5436−5441.
23. Campbell, K. A., Peloquin, O. M., Diner, B. A., Tang, X.-S., Chrisholm, D. A., and Britt, R. D. (1997) *J. Am. Chem. Soc. 119*, 4787−4788.
24. Diner, B. A., Nixon, P. J., and Farchaus, J. W. (1991) *Curr. Opin. Struct. Biol. 1*, 546−554.
25. Roffey, R. A., van Wijk, K. J., Sayre, R. T., and Styring, S. (1994) *J. Biol. Chem. 269*, 5115−5121.
26. Chu, H.-A., Nguyen, A. P., and Debus, R. J. (1995) *Biochemistry 34*, 5839−5858.
27. Mäntele, W. (1993) *Trends Biochem. Sci. 18*, 197−202.
28. Berthomieu, C., Nabedryk, E., Mäntele, W., and Breton, J. (1990) *FEBS Lett. 269*, 363−367.
29. Nabedryk, E., Andrianambinintsoa, S., Berger, G., Leonhard, M., Mäntele, W., and Breton, J. (1990) *Biochim. Biophys. Acta 1016*, 49−54.
30. Berthomieu, C., Nabedryk, E., Breton, J., and Boussac, A. (1992) in *Research in Photosynthesis* (Murata, N., Ed.) Vol. II, pp 53−56, Kluwer Academic Publishers, Dordrecht, The Netherlands.
31. Hienerwadel, R., and Berthomieu, C. (1995) *Biochemistry 34*, 16288−16297.
32. Hienerwadel, R., Boussac, A., Breton, J., and Berthomieu, C. (1996) *Biochemistry 35*, 115447−115460.
33. Rögner, M., Nixon, P. J., and Diner, B. A. (1990) *J. Biol. Chem. 265*, 6189−6196.
34. Williams, J. G. K. (1988) *Methods Enzymol. 167*, 766−778.
35. Rippka, R., Deruelles, J., Waterbury, J. B., Herdman, M., and Stanier, R. Y. (1979) *J. Gen. Microbiol. 111*, 1−61.
36. Tang, X.-S., Diner, B. A., Larsen, B. S., Gilchrist, M. L., Jr., Lorigan, G. A., and Britt, D. (1994) *Proc. Natl. Acad. Sci. U.S.A. 91*, 704−708.
37. Noguchi, T., Ono, T., and Inoue, Y. (1992) *Biochemistry 31*, 5953−5956.
38. Diner, B. A., Tang, X.-S., Zheng, M., Dismukes, G. C., Force, D. A., Randall, D. W., and Britt, R. D. (1995) in *Photosynthesis: from Light to Biosphere*, (Mathis, P., Ed.) Vol. II, pp 229−234, Kluwer Academic Publishers, Dordrecht, The Netherlands.
39. Venyaminov, S. Y., and Kalnin, N. N. (1990) *Biopolymers 30*, 1259−1271.
40. Venyaminov, S. Y., and Kalnin, N. N. (1990) *Biopolymers 30*, 1243−1257.
41. Dollinger, G., Eisenstein, L., Lin, S. -L., Nakanishi, K., and Termini, J. (1986) *Biochemistry 25*, 6524−6533.
42. Pitzer, K. S., and Scott, D. W. (1943) *J. Am. Chem. Soc. 65*, 803.
43. Dollish, F. R., Fateley, W. G., and Bentley, F. F. (1974) *Characteristic Raman Frequencies of Organic Compounds*, pp 162−190, Wiley and Sons, New York.
44. Green, J. H., S., Harrison, D. J., and Kynaston, W. (1971) *Spectrochim. Acta 27A*, 2199−2217.
45. Jakobsen, R. J. (1965) *Spectrochim. Acta 21*, 433−442.
46. Takeuci, H., Watanabe, N., and Harada, I. (1988) *Spectrochim. Acta 44A*, 749−761.

47. Socrates, G. (1994) *Infrared characteristic group frequencies*, Wiley, New York.
48. Asher, S. A., Ludwig, M., and Johnson, C. R. (1986) *J. Am. Chem. Soc. 108*, 3186−3197.
49. Lee, Y.-T. (1997) *J. Raman Spectrosc. 28*, 45−51.
50. Ashikawa, I., and Itoh, K., (1979) *Biopolymers 18*, 1859−1876.
51. MacDonald, G. M., Bixby, K. A., and Barry, B. A. (1993) *Proc. Natl. Acad. Sci. U.S.A. 90*, 11024−11028.
52. Bernard, M. T., MacDonald, G. M., and Barry, B. A.(1995) *J. Biol. Chem. 270*, 1589−1594.
53. Steenhuis, J. J., and Barry, B. A. (1996) *J. Am. Chem. Soc. 118*, 11927−11932.
54. Steenhuis, J. J., and Barry, B. A. (1997) *J. Phys. Chem. B 101*, 6652−6660.
55. Cummings, D. L., and Wood, J. L. (1974) *J. Mol. Struct. 20*, 1−40.
56. Takeuci, H., Watanabe, N., Satoh, Y., and Harada, I. (1989) *J. Raman Spectrosc. 20*, 233−237.
57. Dorval, C., and Zeegers-Huyskens, Th. (1973) *Spectrochim. Acta 29A*, 1805−1814.
58. Muller, J. -P., Maes, G., and Zeegers-Huyskens, T. (1974) *J. Chim. Phys. 71*, 893−898.
59. Hall, A., and Wood, J. L. (1967a) *Spectrochim. Acta 23A*, 1257−1266.
60. Wakisaka, A., Yamamoto, Y., Akiyama, Y., Takeo, H., Mizukami, F., and Sakaguchi, K., (1996) *J. Chem. Soc., Faraday Trans. 92*, 3339−3346.
61. Arnett, E. M., Joris, L., Mitchell, E., Murty, T. S. S. R., Gorrie, T. M., and Schleyer, P. v. R. (1970) *J. Am. Chem. Soc. 92*, 2365−2377.
62. Berthomieu, C., and Boussac, A. (1995) *Biospectroscopy 1*, 187−206.
63. Beck, S. M., and Brus, L. E. (1982) *J. Chem. Phys. 176*, 4700−4704.
64. Johnson, C. R., Ludwig, M., and Asher, S. A. (1986) *J. Am. Chem. Soc. 108*, 905−912.
65. Tripathi, G. N. R., and Schuler, R. H. (1984) *J. Chem. Phys. 81*, 113−121.
66. Tripathi, G. N. R., and Schuler, R. H. (1988) *J. Phys. Chem. 92*, 5129−5133.
67. Mukherjee, A., McGlashen, M. L., and Spiro, T. G. (1995) *J. Phys. Chem. 99*, 4912−4917.
68. Nordlund, P., Sjöberg, B.-M., and Eklund, H. (1990) *Nature 345*, 593−598.
69. Bender et al. (1989) *J. Am. Chem. Soc. 111*, 8076−8083.
70. Un, S., Atta**,** M., Fontecave, M., and Rutherford, A. W. (1995) *J. Am. Chem. Soc. 117*, 10713−10719.
71. Fasanella, E. L., and Gordy, W. (1969) *Proc. Natl. Acad. Sci. U.S.A. 62*, 299−304.
72. Backes, G., Sahlin, M., Sjöberg, B.-M., Loehr, T. M., and Sanders-Loehr, J. (1989) *Biochemistry 28*, 1923−1929.
73. Qin, Y., and Wheeler, R. (1995) *J. Chem. Phys. 102*, 1689−1698.
74. Qin, Y., and Wheeler, R. A. (1995) *J. Am. Chem. Soc. 117*, 6083−6092.
75. Svensson, B., Etchebest, C., Tuffery, P., van Kan, P., Smith, J., and Styring, S. (1996) *Biochemistry 35*, 14486−14502.
76. Breton, J., Hienerwadel, R., and Nabedryk, E. (1997) in *Spectroscopy of Biological Molecules: Modern Trends* (Carmona, P., Navarro, R., and Hernanz, A., Eds.) pp 101−102, Kluwer Academic Publishers, Dordrecht, The Netherlands.
77. Breton, J., Nabedryk, E., Allen, J. P., and Williams, J. C. (1997) *Biochemistry 36*, 4515−4525.

BI971521A